SEDIMENTOLOGY the journal of the International Association of Sedimentologists

Sedimentology (2017) **64**, 215–230 doi: 10.1111/sed.12321

Early Jurassic North Atlantic sea-surface temperatures from TEX_{86} palaeothermometry

STUART A. ROBINSON*, MICHA RUHL*, DAVID LEE ASTLEY*, B. DAVID A. NAAFS†, ALEXANDER J. FARNSWORTH‡, PAUL R. BOWN§, HUGH C. JENKYNS*, DANIEL J. LUNT‡, CHARLOTTE O'BRIEN*[1], RICHARD D. PANCOST† and PAUL J. MARKWICK¶

**Department of Earth Sciences, University of Oxford, South Parks Road, Oxford, OX1 3AN, UK (E-mail: stuart.robinson@earth.ox.ac.uk)*

†Organic Geochemistry Unit, School of Chemistry and Cabot Institute, Cantock's Close, University of Bristol, Bristol, BS8 1TS, UK

‡School of Geographical Sciences and Cabot Institute, University of Bristol, University Road, Bristol, BS8 1SS, UK

§Department of Earth Sciences, University College London, Gower Street, London, WC1E 6BT, UK

¶Getech Plc, Kitson House, Elmete Hall, Elmete Lane, Leeds, LS8 2LJ, UK

Associate Editor – Ulrich Heimhofer

ABSTRACT

Early Jurassic marine palaeotemperatures have been typically quantified by oxygen-isotope palaeothermometry of benthic and nektonic carbonate and phosphatic macrofossils. However, records of Early Jurassic sea-surface temperatures that can be directly compared with general circulation model simulations of past climates are currently unavailable. The TEX_{86} sea-surface temperature proxy is based upon the relative abundance of glycerol dialkyl glycerol tetraethers preserved in organic-carbon-bearing sediments. This proxy has been used extensively on Cretaceous and Cenozoic materials and, in one study, on Middle and Upper Jurassic sediments. Here, TEX_{86} is applied, for the first time, to Lower Jurassic (Sinemurian–Pliensbachian) sediments cored at Deep Sea Drilling Project Site 547 in the North Atlantic. The abundance of glycerol dialkyl glycerol tetraethers in these sediments is very low, despite biomarker and Rock-Eval data suggesting that thermal maturity is, generally, low. Sea floor oxygenation and a high input of reworked terrestrially sourced organic matter may explain the low concentrations. For samples from which it was possible to quantify the relative abundance of glycerol dialkyl glycerol tetraethers, TEX_{86} values range from 0·78 to 0·88, equating to sea-surface temperatures in excess of >28°C. These temperatures are broadly comparable with new general circulation model simulations of the Sinemurian and Pliensbachian stages and support the general view of a predominantly warm climate. The new proxy data suggest that, under favourable geological conditions, it is possible to extend the record of TEX_{86}-based sea-surface temperatures back into the Early Jurassic.

Keywords Jurassic, palaeoclimate, Pliensbachian, Sinemurian, SSTs, TEX_{86}.

[1]Present address: Department of Geology and Geophysics, Yale University, 210 Whitney Avenue, New Haven, CT 06511, USA

INTRODUCTION

Although there is a consensus that the Mesozoic Era was characterized predominantly by warm 'greenhouse climates' (e.g. Fischer, 1981; Frakes & Francis, 1988; Frakes *et al.*, 1992), the spatial and temporal variability in climate during the Mesozoic is, generally, uncertain. The abundance of available records and the variety of proxies also tends to decrease with increasing age, such that there are relatively more data available for the Cretaceous than the Jurassic Period. These factors limit the understanding of past climate dynamics and sensitivity, particularly during intervals of major environmental change, and hinder the ability to compare the geological record with General Circulation Model (GCM) simulations of past climates. Many studies have compiled oxygen-isotope records from carbonate and phosphate fossils to reconstruct Mesozoic temperatures and temperature trends (e.g. Veizer *et al.*, 1999; Jenkyns *et al.*, 2002; Pucéat *et al.*, 2003; Prokoph *et al.*, 2008; Dera *et al.*, 2011; Friedrich *et al.*, 2012; Price *et al.*, 2013; Korte *et al.,* 2015). However, interpretation of these datasets can be complicated by a number of modifying factors including diagenesis, uncertainties regarding the oxygen-isotopic composition of local and global seawater, and the palaeoecology and physiology of the organism used (for example, the water depth inhabited by the organism, geographic and water depth migration, ontogeny and 'vital effects').

Reconstructing sea-surface temperatures (SSTs) for the geological past allows spatial and temporal palaeoclimatic variability to be investigated and directly compared with palaeoclimate simulations generated by General Circulation Models (GCMs). For the Cenozoic, numerous SST reconstructions have been generated, based on a wide range of proxies, including the geochemistry ($\delta^{18}O$ or Mg/Ca ratios) of planktonic foraminifera or the alkenone unsaturation index ($U^{K'}_{37}$). Although planktonic foraminifera become relatively abundant in the fossil record in the Middle Jurassic, at least in the European–Atlantic region (e.g. Caron & Homewood, 1983; Hart *et al.*, 2002), their palaeoceanographic utility is limited to the mid-Cretaceous onwards when they become more abundant and with suitable preservation for geochemical studies (e.g. Leckie, 1989). Similarly, the oldest known alkenones are of Early Cretaceous age (Brassell & Dumitrescu, 2004), but their preservation is insufficient in Mesozoic sediments investigated to date to allow reconstruction of SSTs and the application of $U^{K'}_{37}$ is therefore limited to the last *ca* 55 Myr (Brassell, 2014). Hence, to reconstruct SSTs prior to the mid-Cretaceous, other proxies must be sought and tested.

Another approach for reconstructing SSTs is the TetraEther indeX of tetraethers consisting of 86 carbon atoms ('TEX_{86}') organic palaeothermometer (Schouten *et al.*, 2002, 2003, 2013). Isoprenoid glycerol dialkyl glycerol tetraethers (isoGDGTs) are membrane lipids produced by Archaea with varying numbers of cyclopentane rings and, in the case of crenarchaeol and its regioisomer, a cyclohexane ring. Culture studies show that with increasing temperature the relative abundance of isoGDGTs containing higher numbers of cyclopentane rings increases, as does the relative abundance of the regioisomer of crenarchaeol (reviewed in Schouten *et al.*, 2013); this is captured in the TEX_{86} ratio (Schouten *et al.*, 2002). Marine core-top studies suggest that TEX_{86} best correlates with mean annual sea-surface temperature (e.g. Kim *et al.*, 2010), although it is widely acknowledged that the depth interval of maximum isoGDGT production is not the sea surface itself and that the timing of peak production during a year is not consistent globally (reviewed in Schouten *et al.*, 2013; Taylor *et al.*, 2013): TEX_{86} has been used to reconstruct SSTs through much of the Cenozoic and Cretaceous (e.g. Littler *et al.*, 2011; Linnert *et al.*, 2014) and, in one study, has been applied to immature Middle and Upper Jurassic sediments (Jenkyns *et al.*, 2012). In order to extend the TEX_{86} record to other Jurassic sites, it is necessary to identify organic-carbon-bearing sediments of low thermal maturity. Artificial maturation studies showed that the concentration of GDGTs within a sample and the TEX_{86} ratio decrease rapidly with increased thermal maturation, while naturally thermally mature sedimentary rocks are devoid of GDGTs (Schouten *et al.*, 2004, 2013). In the study presented here, the occurrence of isoGDGTs is reported from Lower Jurassic (Sinemurian–Pliensbachian, *ca* 191 Ma) sediments using samples from Deep Sea Drilling Project (DSDP) Site 547 in the subtropical North Atlantic. Consideration of the thermal maturity of the organic matter and the distributions of isoGDGTs allows the first reconstruction of TEX_{86}-based SSTs in sediments of this age, which are then compared with new GCM simulations for the Sinemurian and Pliensbachian. Importantly, the new data demonstrate

the potential of TEX_{86} for reconstructing SSTs in sediments much older than the Cretaceous, provided that depositional and diagenetic conditions were favourable for preservation and thermal maturity is low. Furthermore, the new model and proxy results provide palaeoclimate insights into an interval of the Jurassic that has not been simulated by climate models with modern, IPCC-class GCMs (cf. Chandler *et al.*, 1992).

MATERIALS

Deep Sea Drilling Project (DSDP) Site 547 is located in the Atlantic Ocean, off the Moroccan coast (Fig. 1A) and provides a discontinuous sedimentary record from the uppermost Triassic to Quaternary (Shipboard Scientific Party, 1984). During the Early Jurassic, the site was located on the margins of the proto-North Atlantic basin, which, during the Hettangian–Sinemurian (*ca* 201 to 191 Ma), was a large, low-latitude marine embayment connected only to the Tethys Ocean and north-west European shelf (e.g. Ziegler, 1990; Fig. 1B). The so-called 'Hispanic Corridor', connecting the Tethys Ocean with Panthalassa in the west, opened during the Sinemurian–Pliensbachian transition (*ca* 191 Ma), but only widened, with large-scale migration of faunas between the Tethyan and Pacific realms around the Pliensbachian–Toarcian transition (*ca* 183 Ma; Aberhan, 2001; Porter *et al.*, 2013).

At Site 547, three wells were cored, of which only Hole 547B penetrated Lower Jurassic sediments (Fig. 2). The oldest sediments recovered in Hole 547B (below 932·5 metres below sea floor; mbsf) were sandy mudstones containing gypsum veins with rare dolomite that were interpreted as being deposited in a non-marine environment and dated as Rhaetian–Hettangian (Shipboard Scientific Party, 1984). Between 932·5 mbsf and 846·0 mbsf in Hole 547B (most of lithological Subunit VIB; Shipboard Scientific Party, 1984), a diversity of sediment types were recovered and dated as Early Jurassic. The basal portion of this interval (932·5 to 891·0 mbsf) is a complex mixture of lithologies including mudstones, nodular limestones, limestones and dolomitic breccias. At the base (Hole 547B, cores 23 and 24) a laminated micrite resembling a stromatolite and breccias of stromatolite occur that could represent tidal-flat deposits (Winterer & Hinz, 1984). The overlying sediments were interpreted as being deposited in a pelagic, marine environment (radiolaria and calcareous nannofossils are present) with water depths of *ca* 100 m and influenced by down-slope transport (Winterer & Hinz, 1984). Between 891 and 846 mbsf, the sediments are interbedded claystones and nodular micritic limestones that were deposited in a pelagic environment, with less influence from downslope transport. Importantly, relatively immature, organic-carbon-rich sediments generally bearing 0·5 to 2·0% total organic carbon (TOC) have been reported (e.g. Shipboard Scientific Party, 1984). Samples were taken from cores 23 to 15 from Hole 547B with an emphasis on fine-grained, hemipelagic sediments. Lower Jurassic breccias and Middle–Upper Jurassic pelagic limestones recovered above 846 mbsf were not sampled due to their

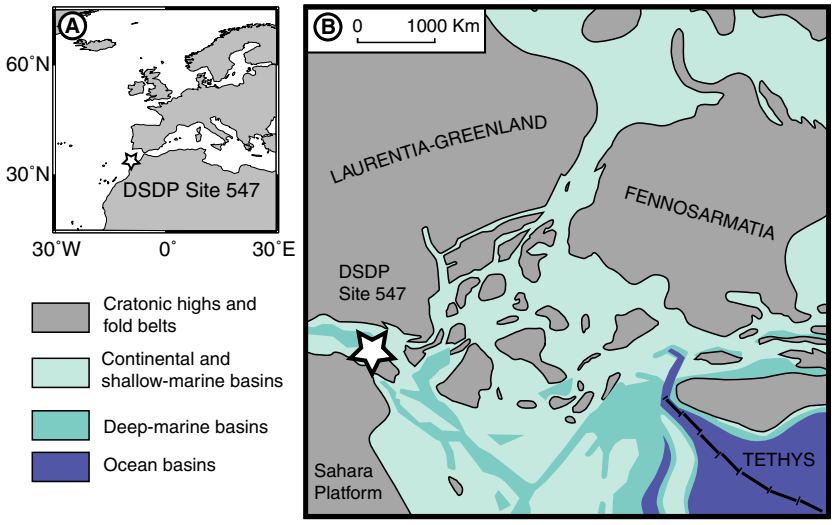

Fig. 1. (A) Present-day map showing the location of DSDP Site 547 (as indicated by the star). Generated using the ODSN Plate Tectonic Reconstruction Service (http://www.odsn.de/odsn/services/paleomap/paleomap.html). (B) Sinemurian–Toarcian palaeogeographic reconstruction of Europe, northern Africa and part of North America showing the location of DSDP Site 547 (as indicated by the star). Adapted from Ziegler (1990).

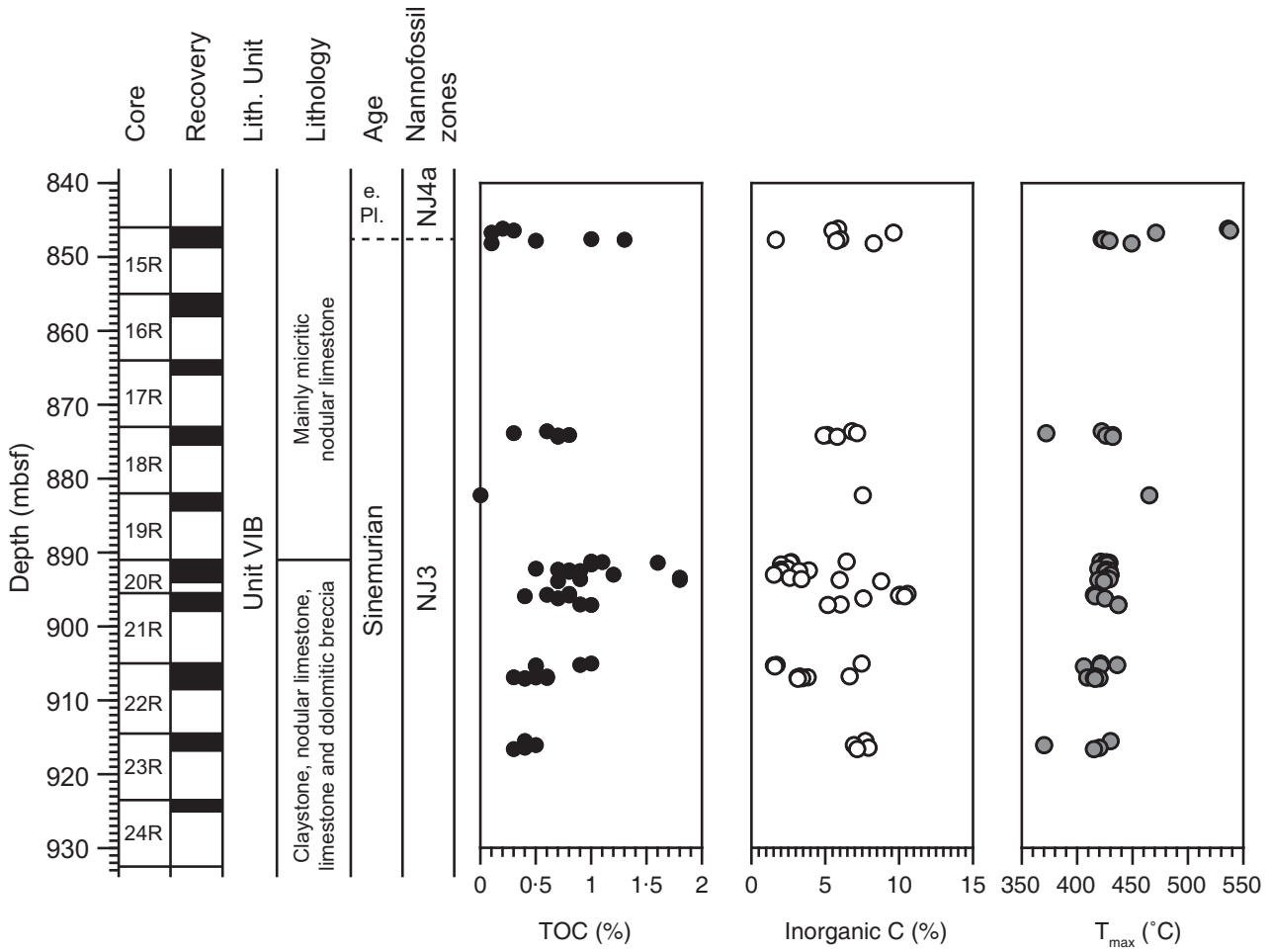

Fig. 2. Core recovery and stratigraphy of Hole 547B and total organic carbon (TOC), inorganic carbon and T_{max} data. e.Pl. = early Pliensbachian.

extremely low TOC contents (Shipboard Scientific Party, 1984) and likely unsuitability for organic geochemistry.

METHODS

Nannofossil biostratigraphy

Calcareous nannofossils were analysed using simple smear slides and standard light microscope techniques (e.g. Bown & Cooper, 1998). Data were collected semi-quantitatively using a Zeiss photomicroscope (Carl Zeiss AG, Oberkochen, Germany) at ×1000 magnification. Abundance and preservation categories are given in Table S1. Biostratigraphy is described with reference to the Jurassic NJ zones of Bown & Cooper (1998) and age calibrations for individual biohorizons are sourced from Gradstein *et al.* (2012)/Time Scale Creator 6.1, unless stated otherwise.

Rock-Eval pyrolysis

Rock-Eval analysis was performed with the Rock-Eval VI unit from Vinci Technologies (Nanterre, France), at the Department of Earth Sciences, University of Oxford. Samples were homogenized and *ca* 50 mg of sample was subsequently analysed by heating (with incremental temperature increases from room temperature to up to 850°C) in the oxidation and pyrolysis ovens. Mineral carbon content was calculated from the $S3_{MINC}$ and S5 peaks, resulting from the CO and CO_2 flux from the sample and analysed by infrared detector. The TOC content was simultaneously obtained in the same sample-run and was calculated from the combined CO and CO_2 fluxes representing the Pyrolysable Carbon

(PC: S1 + S2 + $S3_{CO}$ + $S3_{CO_2}$) and the Residual Carbon (RC: $S4_{CO}$ + $S4_{CO_2}$). Precision and accuracy of the Rock-Eval analyses was checked by regular measurement of the in-house standard SAB134 (a Lower Jurassic shale) and the international reference standard IFP160000. Repeated long-term analyses of the mineral carbon content of SAB134 yields a standard deviation of better than ±0·37%. The long-term analyses of IFP160000 yield an average mineral carbon content of 3·20%, with a standard deviation of 0·02%, within error of the referenced value (3·26 ± 0·12%). For TOC, repeated analyses of SAB134 yields a standard deviation of better than ±0·39%. The long-term average TOC value of IFP160000 is 3·27%, with a standard deviation of 0·04% (again within error of the reported value of 3·28 ± 0·14%). During the measurement of the samples from Site 547, 20 analyses of the in-house SAB134 standard indicate standard deviations of ±0·06% for TOC, 0·08% for mineral carbon-content, ±8 mgHC/gTOC for hydrogen indices (HI), ±2·8 $mgCO_2$/gTOC for oxygen indices (OI), and ±1·7°C for T_{max}.

Biomarkers

Approximately 4 to 7 g of powdered sample was ultrasonically extracted using methanol, then dichloromethane (DCM)/methanol (1:1, v/v) and, finally, 100% DCM. All extracts were combined and dried under N_2 at 40°C. Water was removed from the samples by passing the extracts [dissolved in DCM/methanol (3:1, v/v)] over a column containing anhydrous Na_2SO_4. Extracts were split into apolar and polar fractions by column chromatography, using hexane/DCM (9:1, v/v) and DCM/methanol (1:1, v/v) sequentially and Al_2O_3 as the stationary phase. The polar extract was dissolved in hexane/propanol (99:1, v/v) and then filtered through a PTFE (polytetrafluoroethylene) 0·45 μm filter.

The polar extract was analysed at the University of Oxford using high-performance liquid chromatography/atmospheric pressure positive ion chemical ionization mass spectrometry (HPLC/APCI-MS), using an Agilent 1200 series LC, coupled to a G6130A single quadrupole mass spectrometer. The analytical protocol followed was as described in Schouten *et al.* (2007a). The abundance of isoprenoid GDGTs was measured in selective ion monitoring mode (*m/z* 1302, 1300, 1298, 1296, 1292, 1022, 1020, 1018, etc.). Ion peaks of the respective GDGTs were integrated to determine the relative abundance of each compound. The abundances of the isoGDGTs were used to determine the TEX_{86} value using Eq. 1:

$$TEX_{86} = \frac{\text{GDGT-2} + \text{GDGT-3} + \text{Cren}'}{\text{GDGT-1} + \text{GDGT-2} + \text{GDGT-3} + \text{Cren}'} \quad (1)$$

where Cren′ represents the regioisomer of crenarchaeol. Repeat analysis of an in-house standard following the same analytical sequences as samples reported here suggests an analytical precision on TEX_{86} of ±0·01 (1σ, n = 10).

The apolar fractions were re-dissolved in 10 to 50 μL hexane before analysis with a Thermo ISQ series single quadropole gas chromatography-mass spectrometry (GC–MS) system (Thermo Fisher Scientific, Waltham, MA, USA) at the University of Bristol to determine the C_{31} homohopane 17β,21β(H)/[17β,21β(H) + 17β,21α(H) + 17α,21β(H)] ratio (22R + 22S isomers combined), an indicator of the degree of thermal maturity (Mackenzie *et al.*, 1980). After injection of 1 μL onto a Zebron-I non-polar column (50 m × 0·32 mm × 0·10 μm film thickness), the GC oven programme was: 70°C (1 min hold) to 130°C at 20°C min^{-1}, then to 300°C (held 24 min) at 4°C min^{-1}. The mass spectrometer continuously scanned between *m/z* 50 and 650. Hopanes were integrated using *m/z* 191.

Climate modelling

Global climate, including sea-surface temperatures, was simulated using the UK Met Office coupled ocean–atmosphere General Circulation Model HadCM3L version 4.5, configured with Sinemurian and Pliensbachian palaeogeographies. Lunt *et al.* (2016) gives experimental details for an equivalent set of Cretaceous, Palaeocene and Eocene simulations. The Jurassic simulations here are set up identically to those simulations, except for the use of Early Jurassic palaeogeographies and solar constant. In summary, the model has a resolution of 3·75° in longitude by 2·5° in latitude, in both the atmosphere and ocean, with 19 vertical levels in the atmosphere and 20 vertical levels in the ocean. The present study used Sinemurian and Pliensbachian palaeogeographies created by Getech Plc, using methods based on those of Markwick & Valdes (2004) and downscaled to the model resolution to produce the topographic and bathymetric boundary conditions required by the model.

Atmospheric CO_2 in the model simulations has a value of 1120 ppm (four times pre-industrial values, 4 × PAL), within the range of CO_2 estimates for the Early Jurassic based upon proxies and carbon-cycle models; as summarized in Breecker *et al.* (2010) and Franks *et al.* (2014). The insolation at the top of the atmosphere (Total Solar Irradiance, TSI) was calculated following Gough (1981), with a modern orbital configuration. Both simulations are run for a total of 1422 model years allowing the model to reach near equilibrium, and the climatic means presented here are calculated from the final 30 years of the simulations. For model-data comparisons, the modern latitude and longitude of Site 547 is rotated back to the Sinemurian and Pliensbachian based on the GETECH plate model, for consistency with the model simulations. Where the rotated site falls on land due to the course resolution of the model, the nearest ocean grid-box on the same latitude is utilized.

RESULTS

Nannofossil biostratigraphy

These results were originally presented in an unpublished PhD thesis (University College London) of Paul Bown (Bown, 1986) and are revised

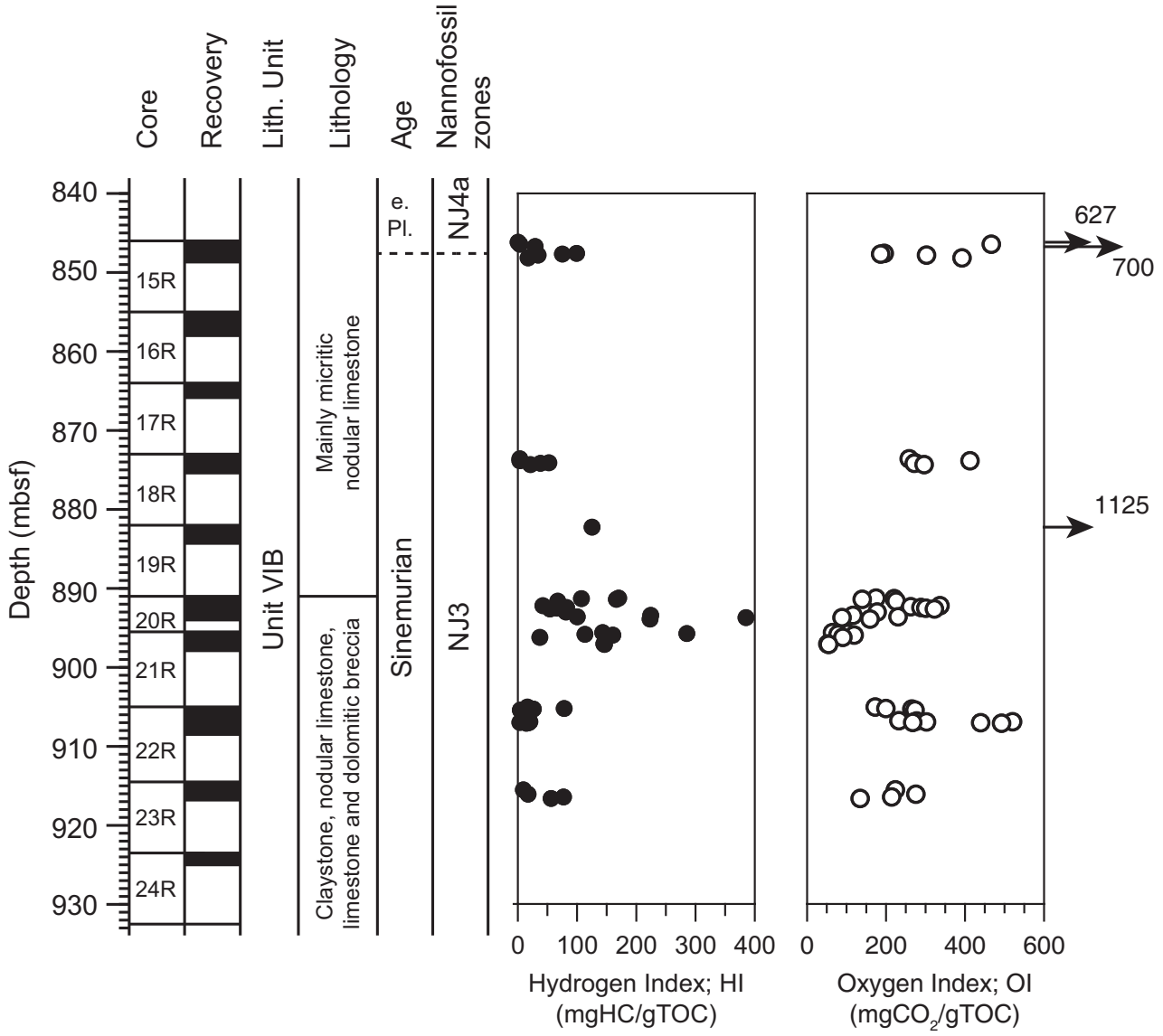

Fig. 3. Core recovery and stratigraphy of Hole 547B and hydrogen index and oxygen index data. e.Pl. = early Pliensbachian.

Table 1. Rock-Eval, C31 homohopanes and TEX_{86} data for selected samples. Where GDGTs were detected and could be quantified, other indices have been calculated: Methane Index (MI), %GDGT-0, and |ΔRI|. BAYSPAR TEX_{86}–SSTs were computed using the default settings for the BAYSPAR model in 'Deep Time' with the exception of the search tolerance which was increased to 3 SD. The 50th percentile values are reported with the 5th and 95th percentiles given in brackets. Linear and TEX_{86}^{H} SSTs were calculated using Eqs 2 and 3 described in the text. Mbsf, metres below sea floor; n.d., not determined; undet., undetected or insufficient GDGTs for determination of TEX_{86}.

Core-section-top (cm)-bottom (cm)	Depth (mbsf)	TOC (%)	Inorganic C (%)	HI	OI	T_{max} (°C)	C31 hopanes $\beta\beta/(\beta\beta+\beta\alpha+\alpha\beta)$	TEX_{86}	MI	%GDGT-0	|ΔRI|	SST – TEX_{86} linear (°C, ±1·7°)	SST – BAYSPAR (5th/95th percentiles)	SST – TEX_{86}^{H} (°C, ±2·5°C)	Comments
Hole 547B															
−15R-2-7-9	847·57	1·0	6·00	99	195	422	0·52	0·78	0·15	3·6	0·3	33·3	28·0 (22·2/33·1)	31·4	Average TEX_{86} reported: n = 4, SD = 0·01
−15R-2-15-17	847·65	1·3	1·64	75	186	424	0·65	0·79	0·16	12·0	0·3	33·7	28·5 (22·7/33·6)	31·6	Average $TEX_{86;}$ reported: n = 4, SD = 0·02
−15R-2-29-32	847·79	0·5	5·74	34	302	429	0·45	0·83	0·13	4·9	0·2	35·7	30·5 (24·6/36·0)	33·0	
−18R-1-110-112	874·10	0·8	5·12	52	273	432	0·62	Undet.							
−18R-1-116-119	874·16	0·7	4·88	38	271	426	0·62	0·88	0·12	2·9	0·1	38·9	33·0 (27·2/38·8)	34·9	
−20R-1-0-3	891·00	n.d.	n.d.	n.d.	n.d.	n.d.	0·56	0·79	0·14	3·9	0·2	33·7	28·6 (22·7/33·8)	31·6	
−20R-1-22-25	891·22	1·0	6·44	170	174	421	0·60	0·83	0·15	3·4	0·1	36·1	30·6 (24·8/36·1)	33·2	
−20R-1-60-62	891·60	1·0	1·99	67	225	427	0·64	Undet.							
−20R-2-0-3	892·50	0·9	3·22	66	300	425	0·65	0·88	0·12	3·7	0·1	38·5	33·0 (27·2/39·0)	34·7	
−20R-2-10-12	892·60	0·8	2·03	54	322	426	0·65	0·83	0·15	6·8	0·2	35·7	30·6 (24·7/35·9)	33·0	Average $TEX_{86;}$ reported: n = 5, SD = 0·02
−20R-2-50-53	893·00	1·2	1·51	81	177	430	0·64	0·85	0·14	10·1	0·1	36·7	31·6 (25·6/37·1)	33·6	
−20R-2-120-122	893·70	1·8	5·96	385	88	419	0·57	Undet.							
−21R-2-10-13	897·10	1·0	5·16	146	54	437	0·00	Undet.							
−22R-2-58-60	907·08	0·4	3·13	14	492	416	0·56	Undet.							
−23R-2-5-7·5	916·05	0·5	6·93	17	275	370	0·51	Undet.							

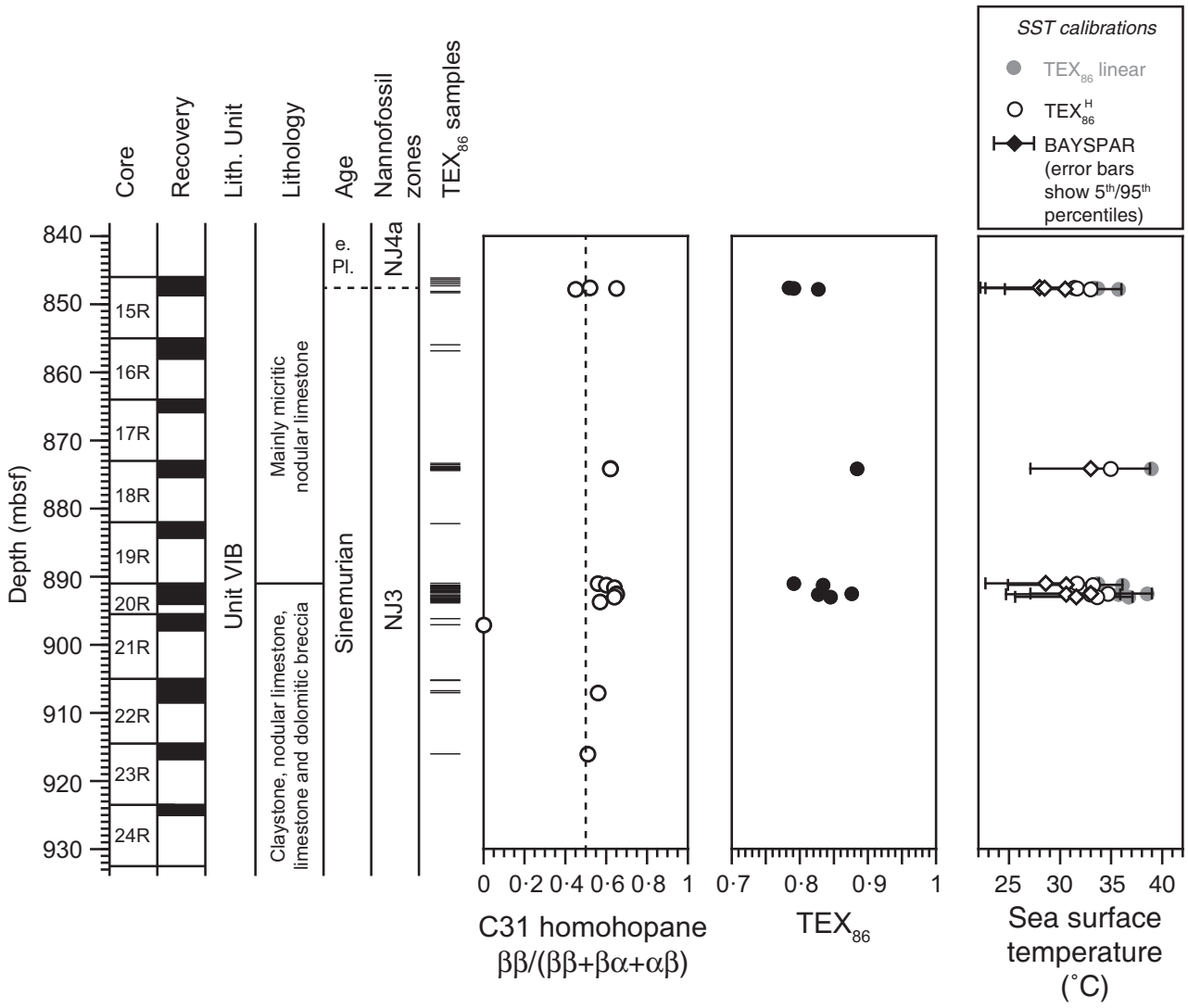

Fig. 4. Core recovery and stratigraphy of Hole 547B with C31 homohopanes and TEX_{86} data, and estimated sea-surface temperatures. The dashed vertical line on the C31 homohopane graph indicates a value of 0·5, above which samples are considered immature enough to yield GDGTs that have not been affected by diagenesis (Schouten *et al.*, 2004). Sea-surface temperatures are calculated using the linear and TEX_{86}^{H} calibrations (Eqs 2 and 3) and BAYSPAR. For visual clarity, error bars for the linear and TEX_{86}^{H} SST calibrations are not shown but are ±1·7 and ±2·5°C, respectively. See text for details. Actual values are provided in Table 1. e.Pl. = early Pliensbachian.

here in light of recent advances in nannofossil biostratigraphy. The presence of *Crepidolithus crassus* and *Orthogonoides hamiltoniae* (Table S1) constrains most of the depth interval studied (below 847·53 mbsf in Hole 547B) to nannofossil Zone NJ3, which is, predominantly, of late Sinemurian age. The lowest occurrence of *Similiscutum cruciulus* at 847·53 mbsf and the presence of *Crepidolithus pliensbachensis* to the top of the section, indicates the presence of the NJ4a subzone of early Pliensbachian age (Bown & Cooper, 1998). The data suggest that the studied sequence falls in the age range 194·3 to 189·0 Ma and is stratigraphically equivalent to the *Oxynoticeras oxynotum*, *Echioceras raricostatum* and *Uptonia jamesoni* ammonite zones, extending across the Sinemurian–Pliensbachian boundary (Gradstein *et al.*, 2012).

Rock-Eval pyrolysis

Results of the Rock-Eval pyrolysis are shown in Figs 2 and 3, and Table S2. Total organic content (TOC) varies from 0 to 1·8%, with a mean of 0·7%

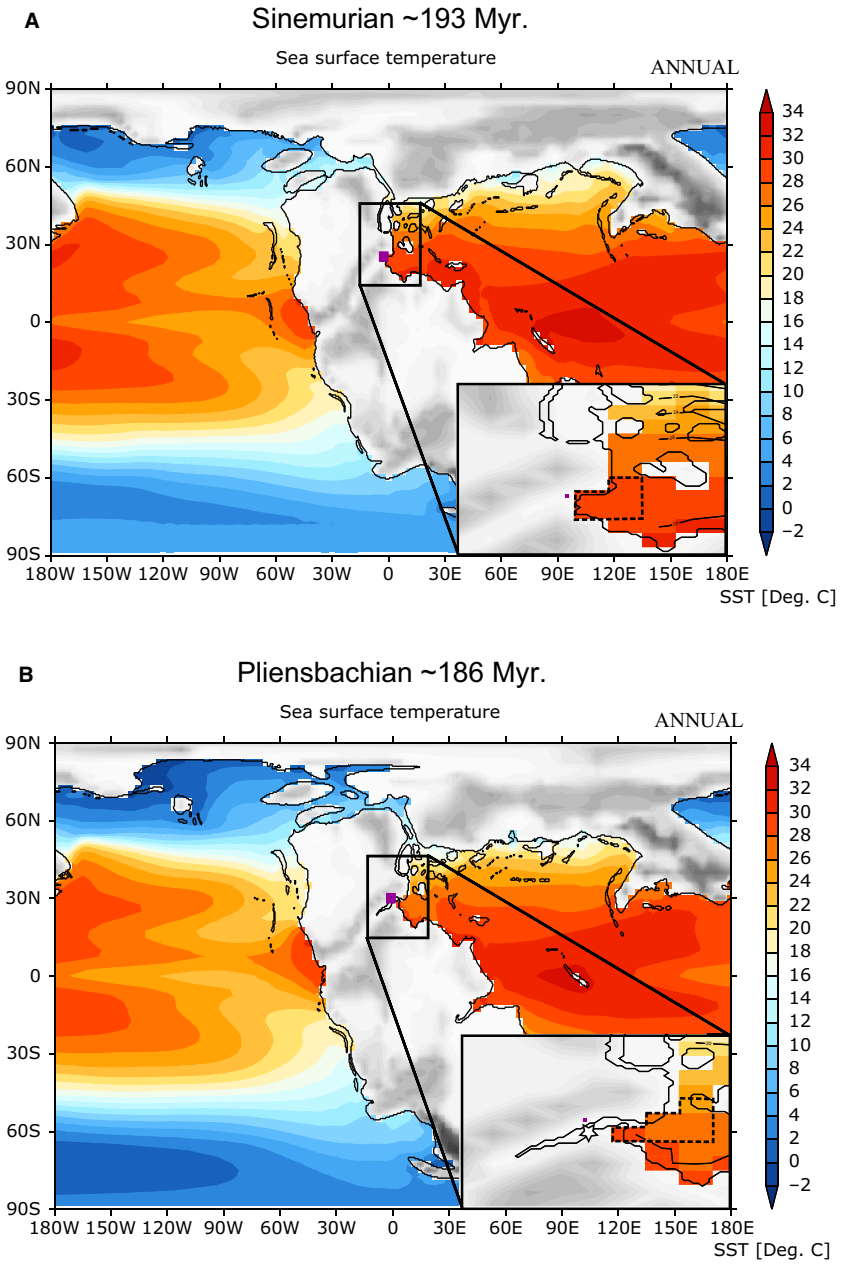

Fig. 5. General circulation model (GCM) simulations of mean annual SST for (A) Sinemurian palaeogeography and (B) Pliensbachian palaeogeography. Model topography is shaded in grey. Insets in both (A) and (B) show the region of interest (15°E–15°W, 15°N–45°N), with the dashed line indicating the area for which mean regional SST is calculated. The purple squares show the centre of the grid square containing Site 547; for clarity in the inset in panel (B) the star shows the likely actual position of Site 547 (cf. Fig. 1).

($1\sigma = \pm 0.4\%$, $n = 49$). There are no clear stratigraphic trends, with most of the variability resulting from changes in lithology between claystones and limestones. Inorganic carbon content varies from 1·5 to 10·6% with a mean of 5·3% ($1\sigma = \pm 2.7\%$, $n = 49$). Due to the presence of both dolomite and calcite (Shipboard Scientific Party, 1984) inorganic carbon content is not converted to $CaCO_3$. The T_{max} values range from 370 to 538°C with an average of 428°C ($1\sigma = \pm 28$°C, $n = 49$). Hydrogen indices (HI) range from 0 to 385 mg HC/gTOC. Oxygen indices (OI) range from 52 to 1125 mg CO_2/gTOC.

Biomarkers

From the polar extracts, it was possible to quantify the abundance of isoGDGTs in nine samples (out of 68 attempted), all of which are Sinemurian in age. In many samples, GDGTs could not be detected or were present at extremely low abundance. Of the nine successful samples, three contained sufficient isoGDGTs to be analysed multiple times (Tables 1 and S3), yielding analytical reproducibilities for TEX_{86} in these three samples of ± 0.01 (1σ, $n = 4$), ± 0.02 (1σ, $n = 5$) and ± 0.02 (1σ, $n = 4$), comparable to the

internal standard analysed in the same analytical sequences (1s = ±0·01, n = 10). The TEX_{86} values of the nine successful samples range from 0·78 to 0·88 (Fig. 4 and Table 1) with an average of 0·83 ± 0·04 (1σ, n = 9). It should be noted that at low concentrations there are likely to be analytical effects on TEX_{86} values (Schouten *et al.*, 2007a), which may lead to an additional source of error (probably less than ±0·1). There is no clear stratigraphic trend in TEX_{86} values but, interestingly, no samples below 894 mbsf yielded sufficient isoGDGTs for quantification of TEX_{86} values. This depth coincides broadly with a lithological change at 891 mbsf (Fig. 4), from sediments containing abundant evidence for downslope transport (below 891 mbsf) to those interpreted as deposited in a hemipelagic environment with limited downslope contributions (above 891 mbsf; Winterer & Hinz, 1984). In every sample analysed, branched GDGTs (brGDGTs) were either below detection limit or insufficiently abundant to be quantified and hence Branched versus Isoprenoid Tetraether index (BIT index; Hopmans *et al.*, 2004) values are not reported.

From the apolar extracts, C31 homohopane $\beta\beta/(\beta\beta + \beta\alpha + \alpha\beta)$ ratios were calculated for all of the samples that yielded isoGDGTS and for six additional samples that did not yield GDGTs. The C31 homohopane $\beta\beta/(\beta\beta + \beta\alpha + \alpha\beta)$ ratios range from 0 to 0·65, with an average of 0·55. Of the 15 samples analysed, the majority (13) have C31 hopane $\beta\beta/(\beta\beta + \beta\alpha + \alpha\beta)$ ratios higher than 0·5 (Fig. 4).

Climate model simulations

Figure 5 shows the modelled annual mean SST for the Sinemurian and Pliensbachian simulations. Globally, the highest SSTs in the Sinemurian and Pliensbachian are 32·5°C and 33·4°C, respectively, and occur in the Tethyan tropics (Fig. 5). On a regional scale the GCM simulates mean annual SSTs of 29·02°C and 26·97°C for the Sinemurian and Pliensbachian, respectively (quoted values are the mean of all ocean grid squares directly surrounding the nearest grid square to Site 547; Fig. 5). One difficulty in determining the modelled temperature for the location of Site 547 is that the palaeogeographic reconstructions have too coarse a geography to be able to represent the intricate archipelago and semi-restricted basin configuration depicted in Fig. 1. For both simulations, this complication may have a bearing on the estimated SSTs because they will be formed under local oceanographic conditions different from those that existed in reality. Sub-grid scale processes within the (semi-) restricted North Atlantic may have had a large dynamical control on local SSTs.

DISCUSSION

Maturity of the organic matter

Schouten *et al.* (2004) demonstrated in artificial maturation experiments that increasing thermal maturity results in lower TEX_{86} values (due to preferential loss of isoGDGTs containing two or more cyclopentane rings) and lower total abundances of isoGDGTs. With sufficient burial, thermal maturity increases to a level at which all isoGDGTs are lost. Thus, before interpreting the TEX_{86} data from Site 547 it is important to consider the thermal maturity of the organic matter, especially given the age of the materials and the observation that many samples did not yield quantifiable amounts of isoGDGTs. The majority of samples analysed by Rock Eval (41 of 49) have T_{max} values <435°C (Fig. 2), indicating that the organic matter is broadly immature. Three samples between *ca* 847 to 846 mbsf have exceptionally high T_{max} values >470°C, suggesting that they are extremely mature. Because these samples occur at the shallowest burial depths of the sample set, it could suggest that reworked, more mature, organic matter is present in these samples. Many of the samples with high T_{max} values are also characterized by high OI values (Fig. 3), indicating that the organic matter is very oxidized, which could also indicate an allochthonous origin. Unsurprisingly, these samples did not yield GDGTs. The GDGTs were only recovered from samples with T_{max} values <430°C (Table 1). The C31 homohopane $\beta\beta/(\beta\beta + \beta\alpha + \alpha\beta)$ ratios of >0·5 in most GDGT-bearing samples support the interpretation of low-maturity organic matter and suggest that the TEX_{86} values reported here have not been compromised by catagenesis (Schouten *et al.*, 2004). The one sample analysed with a C31 hopane $\beta\beta/(\beta\beta + \beta\alpha + \alpha\beta)$ ratio of 0 (i.e. containing no $\beta\beta$ hopanes) did not yield GDGTs. Intriguingly, many samples did not yield sufficient GDGTs despite being immature as indicated by low T_{max} values and, where available, C31 hopane $\beta\beta/(\beta\beta + \beta\alpha + \alpha\beta)$ ratios >0·5. More biomarker data are required to explore this relationship, but the preliminary findings suggest that

maturity alone cannot explain the abundance of GDGTs in the Lower Jurassic sediments at Site 547. Neither does the presence or absence of GDGTs seem to be related to TOC; successful sediments span a range of TOC contents from 0·5 to 1·8%, and some high-TOC sediments did not contain detectable GDGTs. The low HI-values and moderate OI-values of the GDGT-bearing samples suggest that the organic matter is predominantly from a terrigenous source (Type III) or is partially oxidized, as previously suggested by Rullkötter *et al.* (1984). The very low abundances of branched GDGTs from Site 547 suggest that the contribution of soil organic matter to the terrigenous organic matter pool was very low, and that higher plant organic matter supply dominated.

The factors described here and other aspects of the depositional environment (for example, archaeal productivity, bottom-water oxygenation and sedimentation rates; e.g. Schouten *et al.*, 2004; Littler *et al.*, 2014) could have been more important than diagenesis or total rates of organic-matter accumulation in determining the concentration of GDGTs deposited during the Early Jurassic at Site 547. It is important to note that, although there is clear evidence for oxidation of organic matter, oxic degradation is not thought to significantly affect TEX_{86} ratios (see discussion in Schouten *et al.*, 2013). The coincidence between a decrease in the abundance of downslope transport of sediments at *ca* 891 mbsf and the increase in the abundance of GDGTs (as determined by the ability to calculate TEX_{86} ratios) at *ca* 894 mbsf supports a primary oceanographic or depositional control on GDGT preservation and/or abundance.

Other possible factors influencing TEX_{86} values

In addition to diagenesis, other factors, such as contamination by GDGTs sourced from soils (e.g. Weijers *et al.*, 2006) or *in situ* production of GDGTs within the sediment pile by methanogenic and methanotrophic Archaea (e.g. Sinninghe Damsté *et al.*, 2012; Zhang *et al.*, 2011), can affect TEX_{86} values and prohibit their interpretation as a proxy for SSTs. The absence, or extremely low abundances, of branched GDGTs in all samples suggests that the input of soil-sourced GDGTs was extremely low (despite the possible input of terrestrially sourced organic matter: Rullkötter *et al.*, 1984) and, therefore, was not an influencing factor on the TEX_{86} values. *In situ* production of GDGTs by methanogenic and methanotrophic archaea can be assessed through the use of the %GDGT-0 (e.g. Sinninghe Damsté *et al.*, 2012) and the methane index (MI; e.g. Zhang *et al.*, 2011). GDGT-0 (and to a lesser extent GDGT-1, GDGT-2 and GDGT-3) can be synthesized by sedimentary methanotropic Archaea (Koga *et al.*, 1993; Weijers *et al.*, 2006). Using data from culture studies, it has been suggested that if the %GDGT-0 (relative to %Cren) is greater than 67%, there could be an additional, non-water column, source of GDGT-1, GDGT-2 and GDGT-3 (e.g. Sinninghe Damsté *et al.*, 2012), thereby influencing the obtained TEX_{86} value. The %GDGT-0 values for the Site 547 samples are all <15% (Table 1). The methane index (MI) relies upon the observation that normal marine sediments typically have MI values <0·3, whereas sediments influenced by high rates of methane production have values >0·5. The MI values for Site 547 are all <0·2 (Table 1), suggesting marine conditions and a lack of GDGT production by methanotrophs.

Zhang *et al.* (2016) have suggested a new index for assessing the influence of non-thermal factors on TEX_{86} that also identifies data that deviate from modern analogues. The Ring Index (RI) is a weighted average of the cyclopentane moieties and, in the modern core-top dataset, is significantly correlated with TEX_{86}. Zhang *et al.* (2016) suggest that geological samples that deviate from this relationship may not be used for palaeothermometry with confidence, and use the offset between the RI value of a sample and the modern TEX_{86}-RI relationship (termed 'ΔRI') to identify spurious samples, with absolute ΔRI (|ΔRI|) values >0·3. The samples from Site 547 all have |ΔRI| values of ≤0·3 and, therefore, do not seem in any way unusual compared to the modern dataset.

Early Jurassic sea-surface temperatures from DSDP Site 547

The absence of diagenetic or other confounding factors that may have compromised the GDGT distributions measured from Site 547, allows for the use of the TEX_{86} data to reconstruct Sinemurian SSTs for the proto-North Atlantic. The TEX_{86} values from Site 547 are higher than almost all values found anywhere in the modern ocean, with the exception of data from the Red Sea (Kim *et al.*, 2010; Tierney & Tingley, 2015), suggesting that subtropical sea-surface temperatures were as warm, or warmer, than modern

during the Early Jurassic. The low %GDGT-0 provides additional evidence for high SST (i.e. Schouten *et al.*, 2002).

In the modern core-top calibration data, TEX_{86} values from the Red Sea deviate slightly from the modern calibration and yield higher than observed SSTs, possibly due to the presence of a phylogenetically distinct archaeal population (Trommer *et al.*, 2009). For geological samples, it is not yet easy to distinguish between ancient GDGT distributions that were the consequence of warmer than modern SSTs or ancient 'Red Sea-like' populations (e.g. Inglis *et al.*, 2015; Zhang *et al.*, 2015). In the case of many open-ocean records formed during the Cretaceous and Cenozoic it is unlikely that their high TEX_{86} values are the consequence of restricted oceanographic conditions like those found in the modern Red Sea or Mediterranean, which might have led to atypical populations of Thaumarchaeota. However, the North Atlantic Basin in the Early Jurassic would, potentially, have had similarities with those modern basins, because it was situated at low latitudes and likely possessed only a single connection to the global ocean until the Early Pliensbachian (Aberhan, 2001), suggesting that the SSTs calculated from the GDGT data should be treated with some caution. Nonetheless, it is interesting to note that the nannofossil assemblages show relatively high diversities and abundances for this time interval (with the exception of barren samples), that are comparable with other open-marine Tethyan sections, suggesting normal conditions at Site 547 and good connectivity with the 'global' ocean.

A number of approaches exist for calculating SST from TEX_{86} data (Kim *et al.*, 2008, 2010; Schouten *et al.*, 2013; Tierney & Tingley, 2014, 2015) and the different methodologies remain active areas of research and debate. Here, Early Jurassic SSTs are estimated using three approaches, all of which require extrapolation of modern SST–TEX_{86} relationships. Firstly, a linear calibration (Eq. 2; Kim *et al.*, 2008) is used that excludes modern core-top data from the Red Sea:

$$\begin{aligned} &TEX_{86}\ \text{linear SST}(^{\circ}\text{C}) \\ &\quad = 56{\cdot}2 \times (TEX_{86}) - 10{\cdot}78 \\ &\quad (\text{calibration error: } \pm 1{\cdot}7^{\circ}\text{C}) \end{aligned} \qquad (2)$$

Equation 2 is favoured over the linear calibration of Kim *et al.* (2010), because that calibration included cold-water data (<5°C) that may not conform to the linear SST–TEX_{86} relationship observed at warmer temperatures. A linear relationship between TEX_{86} and SST up to 40°C is supported by mesocosm experiments (Schouten *et al.*, 2007b), yet the linear calibrations available (e.g. Kim *et al.*, 2008, 2010) yield very high temperatures at high TEX_{86} values, which some authors consider to be unrealistic (e.g. Hay & Floegel, 2012).

Secondly, a Bayesian model approach is applied, BAYSPAR (Tierney & Tingley, 2014, 2015), that compares measured TEX_{86} values with similar values in the modern core-top dataset to derive linear regression parameters: BAYSPAR fully propagates uncertainties in the core-top data into resulting temperature predictions (Tierney & Tingley, 2014).

Thirdly, a logarithmic calibration (TEX_{86}^{H}, Eq. 3) from Kim *et al.* (2010) is applied, which yields lower estimates of SSTs at high TEX_{86} values than the linear calibration. Although this approach is commonly used in many palaeoclimatic studies, it is not supported by mesocosm studies (reviewed in Schouten *et al.*, 2013) and is associated with structural residuals at high values (Tierney & Tingley, 2014, 2015):

$$\begin{aligned} &TEX_{86}^{H}\ \text{SST}(^{\circ}\text{C}) \\ &\quad = 68{\cdot}4 \times (\log(TEX_{86})) + 38{\cdot}6 \\ &\quad (\text{calibration error: } \pm 2{\cdot}5^{\circ}\text{C}) \end{aligned} \qquad (3)$$

Sinemurian SSTs are estimated (Table 1 and Fig. 4) to be between *ca* 33°C and 39°C using the linear calibration (Eq. 2); *ca* 28° to 32°C using BAYSPAR; and *ca* 31 to 35°C using the logarithmic calibration (TEX_{86}^{H}, Eq. 3). All three calibrations are within error of each other for each sample (Table 1). During the Sinemurian, Site 547 was at a palaeolatitude of *ca* 25°N and it was at *ca* 30°N in the Pliensbachian. Cretaceous and early Cenozoic estimates of SSTs from similar palaeolatitudes, based upon both TEX_{86} and $\delta^{18}O$ of well-preserved planktonic foraminifera, are broadly in the same range (e.g. Forster *et al.*, 2007; Bornemann *et al.*, 2008; Littler *et al.*, 2011; Linnert *et al.*, 2014; Inglis *et al.*, 2015), suggesting that the Early Jurassic SSTs are consistent with those derived for other past greenhouse worlds. North-west European Sinemurian–early Pliensbachian palaeotemperatures of *ca* 15 to 25°C have previously been reconstructed using $\delta^{18}O$ (e.g. Hesselbo *et al.*, 2000; Dera *et al.*, 2009; Suan *et al.*, 2010; Gomez *et al.*,

2016). Given that much of these data come from benthic or nektobenthic organisms (for example, bivalves, belemnites, brachiopods and demersal fish) that record sub-sea-surface environments, and are from higher palaeolatitudes (up to 40°N) than Site 547, a temperature offset between these different datasets and the TEX_{86} data presented here is unsurprising. On the former point, for Cretaceous sediments where it has been possible to measure belemnite $\delta^{18}O$ and TEX_{86} from the same stratigraphic sections deposited in hemipelagic settings, significant offsets of 4 to 14°C have been recorded (e.g. Mutterlose *et al.*, 2010; Jenkyns *et al.*, 2012).

The Early Jurassic SSTs predicted from the nearest grid squares (29°C and 27°C) in the climate model simulations of the Sinemurian and Pliensbachian (Fig. 5) are at the lower end of the range of average values predicted by TEX_{86} (Table 1), The GCM temperatures are within the error margins predicted by BAYSPAR (Table 1). Irrespective of the choice of calibration, the similarity between the TEX_{86} and GCM SSTs suggests that the GCMs provide a favourable approximation of Early Jurassic climates using a pCO_2 level of 1120 ppm (4 × PAL), albeit with slightly lower average SSTs. The differences between the average SSTs calculated by TEX_{86} from Site 547 and the GCM simulations could be due to a number of factors. The complex palaeogeography of the North Atlantic in the Early Jurassic may not be sufficiently well represented in the climate models and may not accurately reproduce ocean circulation on a local scale. Although 1120 ppm is within the range of pCO_2 estimates for the Early Jurassic based upon proxies and carbon-cycle models (summarized in Breecker *et al.*, 2010; Franks *et al.*, 2014), there is potential that CO_2 levels were slightly higher (or lower) than this, which would lead to higher (or lower) SSTs. If additional SST data could be generated for multiple Sinemurian and Pliensbachian localities and palaeolatitudes it would then be possible to determine whether the GCM simulations can reliably predict the correct patterns of SST differences between sites and at what pCO_2 level the GCMs predict the most similar temperatures to those estimated from the geological record.

CONCLUSIONS

The glycerol dialkyl glycerol tetraethers (GDGT) data from Site 547 indicate that, under the right depositional and burial conditions, it is feasible to extract and determine the distributions of these lipids for intervals of geological time much older than previously reported. However, the results here indicate that Site 547 is not an ideal site to reconstruct Early Jurassic sea-surface temperatures (SSTs) by TEX_{86} because there is evidence to suggest that the action of syn-depositional processes, such as bottom-water oxygenation, may have reduced the abundance of GDGTs. Furthermore, it is possible that the Sinemurian North Atlantic was a warm, semi-restricted basin. Because some modern analogues of such basins are characterized by GDGT distributions that deviate slightly from the global TEX_{86}–sea-surface temperature relationships, further work is required to ascertain whether the open-ocean relationships are applicable in this palaeogeographic setting. Nonetheless, the TEX_{86} data indicate that mean sea-surface temperatures in the Early Jurassic were at least as warm as anywhere in the modern ocean and, probably, in excess of 28°C, comparable with similar palaeolatitudes during other intervals of the Cretaceous and Early Cenozoic. The reconstructed temperatures are generally slightly warmer than those indicated by climate-model simulations using an atmospheric CO_2 level four times greater than pre-industrial values, but there are considerable uncertainties regarding Early Jurassic atmospheric pCO_2 levels. Modelling at higher CO_2 concentrations is likely to yield a better fit with the proxy evidence from Site 547.

ACKNOWLEDGEMENTS

We are grateful for funding from NERC (NE/K012479/1 & NE/K014757/1) and the Department of Earth Sciences, University of Oxford. We thank the International Ocean Discovery Program for providing samples and Getech Plc for the palaeogeographic reconstructions used in the climate modelling. Two anonymous reviewers and the Associate Editor, Uli Heimhofer, are warmly thanked for their useful comments.

REFERENCES

Aberhan, M. (2001) Bivalve palaeobiogeography and the Hispanic Corridor: time of opening and effectiveness of a proto-Atlantic seaway. *Palaeogeogr. Palaeoclimatol. Palaeoecol.*, **165**, 375–394.

Bornemann, A., **Norris, R.D.**, **Friedrich, O.**, **Beckmann, B.**, **Schouten, S.**, **Sinninghe Damsté, J.S.**, **Vogel, J.**, **Hofmann, P.** and **Wagner, T.** (2008) Isotopic evidence for glaciation during the Cretaceous supergreenhouse. *Science*, **319**, 189–192.

Bown, P.R. (1986) Taxonomy, biostratigraphy and biogeography of late Triassic to early Jurassic calcareous nannofossils. Unpublished PhD thesis, University College London.

Bown, P.R. and **Cooper, M.K.E.** (1998) Jurassic. In: *Calcareous Nannofossil Biostratigraphy* (Ed. P.R. Bown), pp. 34–85. British Micropalaeontological Society Publication Series. Chapman & Hall, London.

Brassell, S.C. (2014) Climatic influences on the Paleogene evolution of alkenones. *Paleoceanography*, **29**, 255–272.

Brassell, S.C. and **Dumitrescu, M.** and the ODP Leg 198 Shipboard Scientific Party (2004) Recognition of alkenones in a lower Aptian porcellanite from the west-central Pacific. *Org. Geochem.*, **35**, 181–188.

Breecker, D.O., **Sharp, Z.D.** and **McFadden, L.D.** (2010) Atmospheric CO_2 concentrations during ancient greenhouse climates were similar to those predicted for A.D. 2100. *Proc. Natl Acad. Sci.*, **107**, 576–580.

Caron, M. and **Homewood, P.** (1983) Evolution of early planktic foraminifers. *Mar. Micropalaeontol.*, **7**, 453–462.

Chandler, M.A., **Rind, D.** and **Ruey, R.** (1992) Pangean climate during the Early Jurassic: GCM simulations and the sedimentary record of paleoclimate. *GSA Bull.*, **104**, 543–559.

Dera, G., **Pucéat, E.**, **Pellenard, P.**, **Neige, P.**, **Delsate, D.**, **Joachimski, M.M.**, **Reisberg, L.** and **Marinez, M.** (2009) Water mass exchange and variations in seawater temperature in the NW Tethys during the Early Jurassic: evidence from neodymium and oxygen isotopes of fish teeth and belemnites. *Earth Planet. Sci. Lett.*, **286**, 198–207.

Dera, G., **Brigaud, B.**, **Monna, F.**, **Laffont, R.**, **Pucát, E.**, **Deconinck, J.-F.**, **Pellenard, P.**, **Joachimski, M.M.** and **Durlet, C.** (2011) Climatic ups and downs in a disturbed Jurassic world. *Geology*, **39**, 215–218.

Fischer, A.G. (1981) Climatic oscillations in the biosphere. In: *Biotic Crises in Ecological and Evolutionary Time* (Ed. M. Nitecki), pp. 103–131. Academic Press, New York, NY.

Forster, A., **Schouten, S.**, **Baas, M.** and **Sinninghe Damsté, J.S.** (2007) Mid-Cretaceous (Albian–Santonian) sea surface temperature record of the tropical Atlantic Ocean. *Geology*, **35**, 919–922.

Frakes, L. and **Francis, J.** (1988) A guide to Phanerozoic cold polar climates from high-latitude ice-rafting in the Cretaceous. *Nature*, **333**, 547–549.

Frakes, L., **Francis, J.** and **Syktus, J.** (1992) *Climate Modes of the Phanerozoic: The History of the Earth's Climate over the Past 600 Million Years*. Cambridge University Press, Cambridge.

Franks, P.J., **Royer, D.L.**, **Beerling, D.J.**, **van de Water, P.K.**, **Cantrill, D.J.**, **Barbour, M.M.** and **Berry, J.A**. (2014) New constraints on atmospheric CO_2 concentration for the Phanerozoic. *Geophys. Res. Lett.*, **41**, 4685–4694.

Friedrich, O., **Norris, R.D.** and **Erbacher, J.** (2012) Evolution of middle to Late Cretaceous oceans – a 55 my record of Earth's temperature and carbon cycle. *Geology*, **40**, 107–110.

Gomez, J.J., **Comas-Rengifo, M.J.** and **Goy, A.** (2016) Palaeoclimatic oscillations in the Pliensbachian (Lower Jurassic) of the Asturian Basin (Northern Spain). *Clim. Past.*, **12**, 1199–1214.

Gough, D. (1981) Solar interior structure and luminosity variations. *Sol. Phys.*, **74**, 21–34.

Gradstein, F.M., Ogg, J.G., Schmitz, M. and Ogg, G. (eds.) (2012) *The Geological Timescale 2012*. Elsevier, Amsterdam.

Hart, M.B., **Oxford, M.J.** and **Hudson, W**. (2002) The early evolution and palaeobiogeography of Mesozoic planktonic foraminifera. In: *Palaeobiogeography and Biodiversity Change: The Ordovician and Mesozoic-Cenozoic Radiations* (Eds J.A. Crame and A.W. Owen), *Geol. Soc. London. Spec. Publ.*, **194**, 115–125.

Hay, W.W. and **Floegel, S.** (2012) New thoughts about the Cretaceous climate and oceans. *Earth Sci. Rev.*, **115**, 262–272.

Hesselbo, S.P., **Meister, C.** and **Gröcke, D.R.** (2000) A potential global stratotype for the Sinemurian-Pliensbachian boundary (Lower Jurassic), Robin Hood's Bay, UK: ammonite faunas and isotope stratigraphy. *Geol. Mag.*, **171**, 601–607.

Hopmans, E.C., **Weijers, J.W.H.**, **Schefuß, E.**, **Herfort, L.**, **Sinninghe Damsté, J.S.** and **Schouten, S.** (2004) A novel proxy for terrestrial organic matter in sediments based on branched and isoprenoid tetraether lipids. *Earth Planet. Sci. Lett.*, **224**, 107–116.

Inglis, G.N., **Farnsworth, A.**, **Lunt, D.**, **Foster, G.L.**, **Hollis, C.J.**, **Pagani, M.**, **Jardine, P.E.**, **Pearson, P.N.**, **Markwick, P.**, **Galsworthy, A.M.J.**, **Raynham, L.**, **Taylor, K.W.R.** and **Pancost, R.D.** (2015) Descent towards the Icehouse: Eocene sea surface cooling inferred from GDGT distributions. *Paleoceanography*, **30**, 1000–1020.

Jenkyns, H.C., **Jones, C.E.**, **Gröcke, D.R.**, **Hesselbo, S.P.** and **Parkinson, D.N.** (2002) Chemostratigraphy of the Jurassic System: applications, limitations and implications for palaeoceanography. *J. Geol. Soc. London*, **159**, 351–378.

Jenkyns, H.C., **Schouten-Huibers, L.**, **Schouten, S.** and **Sinninghe Damsté, J.S.** (2012) Warm Middle Jurassic-Early Cretaceous high-latitude sea-surface temperatures from the Southern Ocean. *Clim. Past*, **8**, 215–226.

Kim, J.-H., **Schouten, S.**, **Hopmans, E.C.**, **Donner, B.** and **Sinninghe Damsté, J.S.** (2008) Global sediment core-top calibration of the TEX_{86} paleothermometer in the ocean. *Geochim. Cosmochim. Acta*, **72**, 1154–1173.

Kim, J.-H., **van der Meer, J.**, **Schouten, S.**, **Helmke, P.**, **Willmott, V.**, **Sangiorgi, F.**, **Koç, N.**, **Hopmans, E.C.** and **Sinninghe Damsté, J.S.** (2010) New indices and calibrations derived from the distribution of crenarchaeal isoprenoid tetraether lipids: implications for past sea surface temperature reconstructions. *Geochim. Cosmochim. Acta*, **74**, 4639–4654.

Koga, Y., **Akagawa-Matsushita, M.**, **Ohga, M.** and **Nishihara, M.** (1993) Taxonomic significance of the distribution of component parts of polar ether lipids in methanogens. *Syst. Appl. Microbiol.*, **16**, 342–351.

Korte, C., **Hesselbo, S.P.**, **Ullmann, C.V.**, **Dietl, G.**, **Ruhl, M.**, **Schweigert, G.** and **Thibault, N.** (2015) Jurassic climate mode governed by ocean gateway. *Nature Comms.*, **6**, 10015. doi: 10.1038/ncomms10015.

Leckie, R.M. (1989) A paleoceanographic model for the early evolutionary history of planktonic foraminifera. *Palaeogeog. Palaeoclim. Palaeoecol.*, **73**, 107–138.

Linnert, C., **Robinson, S.A.**, **Lees, J.A.**, **Bown, P.R.**, **Pérez-Rodríguez, I.**, **Petrizzo, M.R.**, **Falzoni, F.**, **Littler, K.**, **Arz, J.A.** and **Russell, E.E.** (2014) Evidence for global cooling in

the Late Cretaceous. *Nature Comms.*, **5**, 4194. doi:10.1038/ncomms5194.

Littler, K., **Robinson, S.A.**, **Bown, P.R.**, **Nederbragt, A.J.** and **Pancost, R.D.** (2011) High sea-surface temperatures during the Early Cretaceous Epoch. *Nature Geo.*, **4**, 169–172.

Littler, K., **Robinson, S.A.** and **Bown, P.R.** (2014) An offset in TEX_{86} values between interbedded lithologies: implications for sea-surface temperature reconstructions. *Palaeogeog. Palaeoclim. Palaeoecol.*, **399**, 42–51.

Lunt, D.J., **Farnsworth, A.**, **Loptson, C.**, **Foster, G.L.**, **Markwick, P.**, **O'Brien, C.L.**, **Pancost, R.D.**, **Robinson, S.A.** and **Wrobel, N.** (2016) Palaeogeographic controls on climate and proxy interpretation. *Clim. Past*, **12**, 1181–1198.

Mackenzie, A.S., **Patience, R.L.**, **Maxwell, J.R.**, **Vandenbroucke, M.** and **Durand, B.** (1980) Molecular parameters of maturation in the Toarcian shales, Paris Basin, France—I. Changes in the configurations of acyclic isoprenoid alkanes, steranes and triterpanes. *Geochim. Cosmochim. Acta*, **44**, 1709–1721.

Markwick, P.J. and **Valdes, P.J.** (2004) Palaeo-digital elevation models for use as boundary conditions in coupled ocean-atmosphere GCM experiments: a Maastrichtian (late Cretaceous) example. *Palaeogeog. Palaeoclim. Palaeoecol.*, **213**, 37–63.

Mutterlose, J., **Malkoc, M.**, **Schouten, S.**, **Sinninghe Damsté, J.S.** and **Forster, A.** (2010) TEX_{86} and stable $\delta^{18}O$ paleothermometry of early Cretaceous sediments: implications for belemnite ecology and paleotemperature proxy application. *Earth Planet. Sci. Lett.*, **298**, 286–298.

Porter, S.J., **Selby, D.**, **Suzuki, K.** and **Gröcke, D.** (2013) Opening of a trans-Pangaean marine corridor during the Early Jurassic: insights from osmium isotopes across the Sinemurian-Pliensbachian GSSP, Robin Hood's Bay, UK. *Palaeogeog. Palaeoclim. Palaeoecol.*, **375**, 50–58.

Price, G.D., **Twitchett, R.J.**, **Wheeley, J.R.** and **Buono, G.** (2013) Isotopic evidence for long term warmth in the Mesozoic. *Sci. Rep.*, **3**, 1438. doi:10.1038/srep01438.

Prokoph, A., **Shields, G.A.** and **Veizer, J.** (2008) Compilation and time-series analysis of a marine carbonate $\delta^{18}O$, $\delta^{13}C$, $^{87}Sr/^{86}Sr$, and $\delta^{34}S$ database through Earth history. *Earth Sci. Rev.*, **87**, 113–133.

Pucéat, E., **Lécuyer, C.**, **Sheppard, S.M.F.**, **Dromart, G.**, **Reboulet, S.** and **Grandjean, P.** (2003) Thermal evolution of Cretaceous Tethyan marine waters inferred from oxygen isotope composition of fish tooth enamels. *Paleoceanography*, **18**, 1029. doi:10.1029/2002PA000823.

Rullkötter, J., **Mukhopadhyay, P.K.**, **Schaefer, R.G.** and **Welte, D.H**. (1984) Geochemistry and petrography of organic matter in sediments from Deep Sea Drilling Project Sites 545 and 547, Mazagan Escarpment. In: *Initial Reports, DSDP 79*, pp. 775–806. U.S. Govt. Printing Office, Washington, DC.

Schouten, S., **Hopmans, E.C.**, **Schefuß, E.** and **Sinninghe Damsté, J.S.** (2002) Distributional variations in marine crenarchaeotal membrane lipids: a new tool for reconstructing ancient sea water temperatures? *Earth Planet. Sci. Lett.*, **204**, 265–274.

Schouten, S., **Hopmans, E.C.**, **Forster, A.**, **van Breugel, Y.**, **Kuypers, M.M.** and **Sinninghe Damsté, J.S.** (2003) Extremely high sea-surface temperatures at low latitudes during the middle Cretaceous as revealed by archaeal membrane lipids. *Geology*, **31**, 1069–1072.

Schouten, S., **Hopmans, E.C.** and **Sinninghe Damsté, J.S.** (2004) The effect of maturity and depositional redox conditions on archaeal tetraether lipid palaeothermometry. *Org. Geochem.*, **35**, 567–571.

Schouten, S., **Huguet, C.**, **Hopmans, E.C.**, **Kienhuis, M.V.M.** and **Sinninghe Damsté, J.S.** (2007a) Analytical methodology for TEX_{86} paleothermometry by high-performance liquid chromatography/atmospheric pressure chemical ionization-mass spectrometry. *Anal. Chem.*, **79**, 2940–2944.

Schouten, S., **Forster, A.**, **Panoto, F.E.** and **Sinninghe Damsté, J.S.** (2007b) Towards calibration of the TEX_{86} palaeothermometer for tropical sea surface temperatures in ancient greenhouse worlds. *Org. Geochem.*, **38**, 1537–1546.

Schouten, S., **Hopmans, E.C.** and **Sinninghe Damsté, J.S.** (2013) The organic geochemistry of glycerol dialkyl glycerol tetraether lipids: a review. *Org. Geochem.*, **54**, 19–61.

Shipboard Scientific Party (1984) Site 547. In: *Initial Reports. DSDP, 79*. U.S. Govt. Printing Office, Washington, DC, pp. 223–361.

Sinninghe Damsté, J.S., **Ossebaar, J.**, **Schouten, S.** and **Verschuren, D.** (2012) Distribution of tetraether lipids in the 25-kyr sedimentary record of Lake Challa: extracting reliable TEX_{86} and MBT/CBT palaeotemperatures from an equatorial African lake. *Quatern. Sci. Rev.*, **50**, 43–54.

Suan, G., **Mattioli, E.**, **Pittet, B.**, **Lécuyer, C.**, **Suchéras-Marx, B.**, **Vitor Duarte, L.**, **Philippe, M.**, **Reggiani, L.** and **Martineau, F.** (2010) Secular environmental precursors to Early Toarcian (Jurassic) extreme climate changes. *Earth Planet. Sci. Lett.*, **290**, 448–458.

Taylor, K.W.R., **Huber, M.**, **Hollis, C.J.**, **Hernandez-Sanchez, M.D.** and **Pancost, R.D**. (2013) Re-evaluating modern and Palaeogene GDGT distributions: implications for SST reconstructions. *Global Planet. Change*, **108**, 158–174.

Tierney, J.E. and **Tingley, M.P.** (2014) A Bayesian, spatially-varying calibration model for the TEX_{86} proxy. *Geochim. Cosmochim. Acta*, **127**, 83–106.

Tierney, J.E. and **Tingley, M.P.** (2015) A TEX_{86} surface sediment database and extended Bayesian calibration. *Sci. Data*, **2**, 150029. doi:10.1038/sdata.2015.29.

Trommer, G., **Siccha, M.**, **van der Meer, M.T.J.**, **Schouten, S.**, **Sinninghe Damsté, J.S.**, **Schulz, H.**, **Hemleben, C.** and **Kucera, M.** (2009) Distribution of Crenarchaeota tetraether membrane lipids in surface sediments from the Red Sea. *Org. Geochem.*, **40**, 724–731.

Veizer, J., **Ala, D.**, **Azmy, K.**, **Bruckschen, P.**, **Buhl, D.**, **Bruhn, F.**, **Carden, G.A.F.**, **Diener, A.**, **Ebneth, S.**, **Goddéris, Y.**, **Jasper, T.**, **Korte, C.**, **Pawellek, F.**, **Podlaha, O.G.** and **Strauss, H.** (1999) $^{87}Sr/^{86}Sr$, ^{13}C and ^{18}O evolution of Phanerozoic seawater. *Chem. Geol.*, **161**, 59–88.

Weijers, J.W.H., **Schouten, S.**, **Spaargaren, O.C.** and **Sinninghe Damsté, J.S.** (2006) Occurrence and distribution of tetraether membrane lipids in soils: implications for the use of the TEX_{86} proxy and the BIT index. *Org. Geochem.*, **37**, 1680–1693.

Winterer, E.L. and **Hinz, K.** (1984) The evolution of the Mazagan continental margin: a synthesis of geophysical and geological data with results of drilling during Deep Sea Drilling Project Leg 79, In: *Initial Reports. DSDP, 79*, pp. 893–919. U.S. Govt. Printing Office, Washington, DC.

Zhang, Y.G., **Zhang, C.L.**, **Liu, X.-L.**, **Li, L.**, **Hinrichs, K.-U.** and **Noakes, J.E.** (2011) Methane Index: a tetraether archaeal lipid biomarker indicator for detecting the instability of marine gas hydrates. *Earth Planet. Sci. Lett.*, **307**, 525–534.

Zhang, Y.G., **Pagani, P.** and **Wang, Z.** (2016) Ring index: a new strategy to evaluate the integrity of TEX_{86} paleothermometry. *Paleoceanography*, **31**, 220–232.

Ziegler, P.A. (1990) *Geological Atlas of Western and Central Europe*. Shell Internationale Petroleum Maatschappij B.V, The Hague.

Manuscript received 16 February 2016; revision accepted 19 August 2016

Supporting Information

Additional Supporting Information may be found in the online version of this article:

Table S1. Stratigraphic range chart for calcareous nannofossils from Site 547. Species abundance: A >10/field of view (FOV), C 1-10/FOV, F 1/2-10 FOV, R 1/11-100FOV. Nannofossil zones are after Bown & Cooper (1998).

Table S2. Rock-Eval data.

Table S3. Fractional abundances of isoprenoid GDGTs.